Electronic Structures and Properties of Eight-Coordinate Metal−Polyarsenic Complexes MAs_8^{n-} (M = V, Nb, Ta, Cr, Mo, W, Mn, Tc, Re)

Jun Li*,† and Kechen Wu‡

Department of Chemistry, The Ohio State University, Columbus, Ohio 43210, and the State Key Laboratory of Structural Chemistry, Fujian Institute of Research on the Structure of Matter, Chinese Academy of Sciences, Fuzhou, Fujian 350002, China

Received February 23, 1999

The eight-coordinate early transition metal polyarsenic complexes, MAs_8^{3-} (M = V, Nb, Ta), MAs_8^{2-} (M = Cr, Mo, W), and MAs_8^{-} (M = Mn, Tc, Re), have been studied using density functional theory (DFT). The geometry optimizations of these complexes indicate that in the most stable structures the transition metal atoms are trapped in a crownlike cavity consisting of a zigzag eight-membered ring of As_8 cluster. The scalar-relativistic effects and spin−orbit coupling effects on the electronic structures and energy levels were taken into account. The stabilities of gas-phase MAs_8^{n-} ions and bonding between the As_8 ring and early transition metals are discussed on the basis of population analysis, atomization energies, and decomposition reaction energies. All these complex ions are found to be diamagnetic with notable HOMO−LUMO energy gaps. The vibrational frequencies and infrared absorption intensities of the MAs_8^{n-} series are predicted theoretically. Brief theoretical calculations of the similar MoA_8^{2-} pnictide ions indicate that the analogous P, Sb, and even Bi complexes are likely to be stable, whereas the crownlike MoN_8^{2-} is not a stable complex.

In organometallic chemistry, cyclopolyene and cyclopolyenyl systems of η^n-C_nH_n carbocyclics, such as $C_5H_5^-$, C_6H_6, $C_7H_7^{3-}$, and $C_8H_8^{2-}$, are among the most frequently used ligands for both transition metals and f-block elements.[1−4] Although N atoms are isoelectronic and isolobal to CH groups, η^n-N_n ligands are rare in chemistry largely because of their instability arising from a small resonance energy and a large electron repulsion between lone pairs.[5] As heavier analogues of the C_nH_n and N_n rings, P_n and As_n rings are more stable than the smaller-size N_n rings because of the marked decrease of strain energy.[6−11]

In the past two decades it has been found that As_n rings (n = 3, 5, 6, 7, 8) can act as useful ligands for certain transition metals such as Nb, Mo, and Fe.[12−17] Especially noteworthy is the experimental discovery of a polymer ion $_\infty^1[Rb{\cdot}NbAs_8]^{2-}$ by von Schnering and co-workers.[18] In this one-dimensional chain structure, a beautiful monocyclic, crownlike subunit of η^8-cyclooctaarsenidoniobate(V) trianion $NbAs_8^{3-}$ is present. Recently, the free $MoAs_8^{2-}$ and $NbAs_8^{3-}$ complexes have been synthesized and characterized by Eichhorn et al.,[16] which represents the first isolation of the unique binary transition metal pnictide ions. These pioneering experimental studies have opened a new chapter in main-group element inorganic chemistry.[19] The unusual eight-coordinate structures and remarkable significance of these novel As_8 complexes raise a series of intriguing questions that justify a thorough study of the electronic structure and bonding of these complexes by state-of-the-art theoretical chemistry methods.

Since they can provide reliable geometries, vibrational frequencies, and energetics for organometallic complexes,[20−22] DFT methods were chosen to investigate the geometries, stabilities, and vibrational frequencies of the MAs_8^{n-} ions. The structures were optimized for the MAs_8^{n-} complexes, where the central atoms are all the early transition metals of groups 5, 6, and 7. The electronic structures, bonding properties, and thermodynamic stabilities as well as spin−orbit (SO) effects and vibrational properties of these complexes have been explored. We have also compared the calculated atomization energies and decomposition reaction energies of the MoA_8^{2-} (A = N, P, Sb, or Bi) pnictide ions with that of the $MoAs_8^{2-}$ ion.

† The Ohio State University.
‡ Fujian Institute of Research on the Structure of Matter.

(1) Deganello, G. *Transition Metal Complexes of Cyclic Polyolefins*; Academic Press: London, 1979; Chapter 1.
(2) Green, M. L. H.; Ng, D. K. P. *Chem. Rev.* **1995**, *95*, 439.
(3) Li, J.; Bursten, B. E. *J. Am. Chem. Soc.* **1997**, *119*, 9021.
(4) Dolg, M.; Fulde, P. *Eur. J. Chem.* **1998**, *4*, 200.
(5) Gimarc, B. M.; Zhao, M. *Inorg. Chem.* **1996**, *35*, 3289 and references therein.
(6) Ballone, P.; Jones, R. O. *J. Chem. Phys.* **1994**, *100*, 4941.
(7) von Schnering, H. G.; Bolle, U.; Curda, J.; Peters, K.; Carrillo-Cabrera, W.; Somer, M.; Schultheiss, M.; Wedig, U. *Angew. Chem., Int. Ed. Engl.* **1996**, *35*, 984.
(8) von Schnering, H. G. *Angew. Chem., Int. Ed. Engl.* **1981**, *20*, 33.
(9) Kutzelnigg, W. *Angew. Chem., Int. Ed. Engl.* **1984**, *23*, 272.
(10) Driess, M.; Grützmacher, H. *Angew. Chem., Int. Ed. Engl.* **1996**, *35*, 828.
(11) Gimarc, B. M.; Zhao, M. *Coord. Chem. Rev.* **1997**, *158*, 385.
(12) Rheingold, A. L.; Foley, M. J.; Sullivan, P. J. *J. Am. Chem. Soc.* **1982**, *104*, 4727.
(13) Scherer, O. J. *Angew. Chem., Int. Ed. Engl.* **1985**, *24*, 924.
(14) Di Maio, A. J.; Rheingold, A. L. *Chem. Rev.* **1990**, *90*, 169.
(15) Scherer, O. J.; Blath, C.; Wolmershäuser, G. *J. Organomet. Chem.* **1990**, *387*, C21.
(16) Eichhorn, B. W.; Mattamana, S. P.; Gardner, D. R.; Fettinger, J. C. *J. Am. Chem. Soc.* **1998**, *120*, 9708.
(17) Scherer, O. J. *Angew. Chem., Int. Ed. Engl.* **1990**, *29*, 1104.
(18) von Schnering, H. G.; Wolf, J.; Weber, D.; Ramirez, R.; Meyer, T. *Angew. Chem., Int. Ed. Engl.* **1986**, *25*, 353.
(19) Scherer, O. J. *Acc. Chem. Res.* **1999**, *32*, 751.
(20) Ziegler, T. *Chem. Rev.* **1991**, *91*, 651.
(21) Bauschlicher, C. W., Jr. *Chem. Phys. Lett.* **1995**, *246*, 40.
(22) Li, J.; Bursten, B. E. *J. Am. Chem. Soc.* **1998**, *120*, 11456.

10.1021/ic9902166 CCC: $19.00
Published on Web 03/11/2000

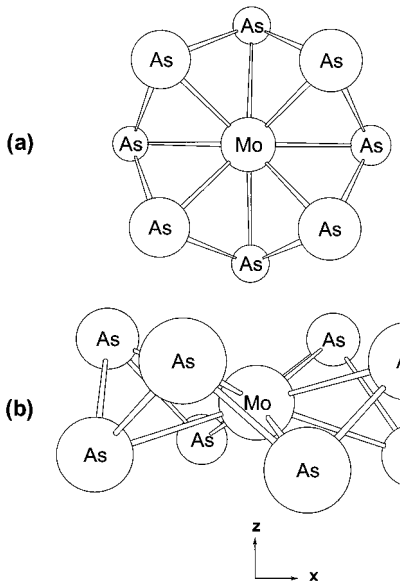

Figure 1. Optimized crownlike configuration of $MoAs_8^{2-}$ ion: (a) top view; (b) side view.

Theoretical Methods

The density functional calculations were performed via a local density approach (LDA)[23,24] and a generalized gradient method by Perdew and Wang (PW91).[25] The scalar relativistic (mass−velocity and Darwin) effects were taken into account by use of the *quasi-relativistic* method.[26] The core orbitals of the arsenic atoms were frozen up to 3p orbitals, while those of the first-, second-, and third-row transition metals were frozen up to 2p, 3d, and 4f orbitals, respectively. Triple-ζ Slater-type-orbital (STO) basis sets were employed for the valence orbitals of all the transition metals and arsenic atoms, with d- and f-type polarization functions for the latter.[27]

Geometries of these complexes were fully optimized by using the analytical energy gradient technique.[28] The frequencies and infrared (IR) absorption intensities were calculated numerically. Inasmuch as the accuracy of a DFT calculation depends not only on error sources encountered in self-consistent field type calculations but also on the number of grid points used in numerical integration of the functionals, tight criteria for numerical integration accuracy (INTEGRATION = 7.0) and gradient convergence (10^{-4}) for geometry optimization and frequency calculations were adopted to reduce numerical noise. All the calculations were carried out using the Amsterdam Density Functional code (ADF 2.1).[29−31]

Results and Discussion

Structures. One of the most important questions regarding these MAs_8^{n-} complexes is "What are their most stable geometries?" Let us take the $MoAs_8^{2-}$ ion as an example to examine the geometries of these complexes. We will focus on the crown configuration (D_{4d}, Figure 1) and the following eight most important isomers of the $MoAs_8^{2-}$ ion: (a) planar configuration (D_{8h} symmetry), (b) cubic configuration (O_h),[32] (c) dodecahedron (DD, D_{2d}), (d) cyclooctatetraene (COT)-shaped configuration (D_{2d}),[33] (e) pentalene-like configuration (C_{2v}), (f) eclipsed sandwich configuration of $M(\eta^4\text{-}As_4)_2$ (D_{4h}), (g) bicapped trigonal prism (BTP, C_{2v}), (h) staggered sandwich configuration of $M(\eta^4\text{-}As_4)_2$ (D_{4d}), as shown in Figure 2.

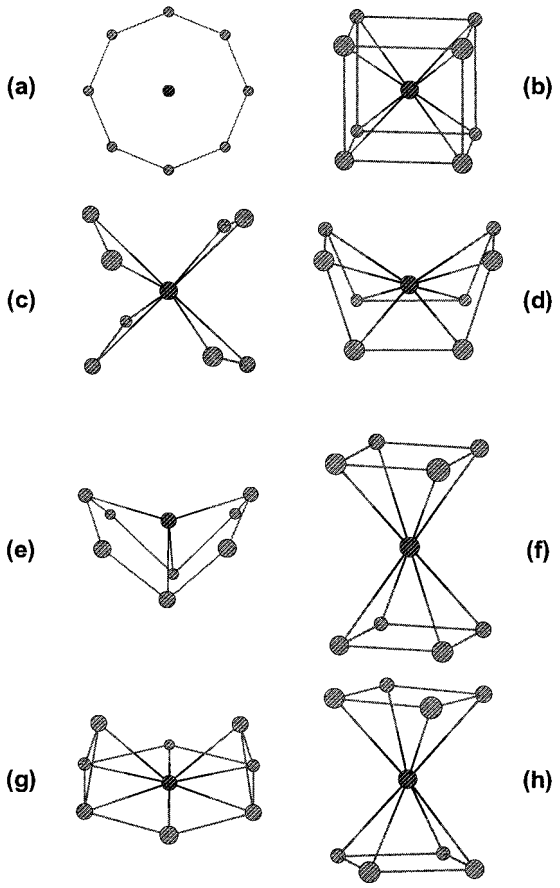

Figure 2. Geometries of eight metastable $MoAs_8^{2-}$ isomers: (a) planar (D_{8h}), (b) cubic (O_h), (c) DD (D_{2d}), (d) cyclooctatetraene-shaped (D_{2d}), (e) pentalene-like (C_{2v}), (f) eclipsed sandwich (D_{4h}), (g) BTP (C_{2v}), (h) staggered sandwich (D_{4d}).

The calculated HOMO−LUMO energy gaps, total energies (with reference to the atomic fragments), and relative energies are listed in Table 1 for these isomers. As expected, the LDA calculations lead to much lower total energies than the PW91 calculations because of the well-known overbinding problem associated with the LDA approximation. The LDA relative energies are also larger than the PW91 ones. The crown configuration, which corresponds to a compressed square antiprism (SAP) in traditional stereochemistry terminology,[34] is found to be the most stable isomer among the nine geometries considered. The other isomers are higher in energy by more than 37 kcal/mol.

From the PW91 calculations, the HOMO−LUMO energy gaps for the crown, BTP, and staggered sandwich configurations of $MoAs_8^{2-}$ ion are 1.64, 1.36, and 0.89 eV, respectively. Frequency calculations indicate that these three configurations correspond to real minima on the potential energy surface. In

(23) Slater, J. C. *Quantum Theory of Molecular and Solids*; McGraw-Hill: New York, 1974; Vol. 4.
(24) Vosko, S. H.; Wilk, L.; Nusair, M. *Can. J. Phys.* **1980**, *58*, 1200.
(25) Perdew, J. P.; Wang, Y. *Phys. Rev.* **1992**, *B45*, 13244.
(26) Ziegler, T.; Baerends, E. J.; Snijder, J. G.; Ravenek, W. *J. Phys. Chem.* **1989**, *93*, 3050.
(27) Vernooijs, P.; Snijder, G. J.; Baerends, E. J. *Slater Type Basis Functions for the Whole Periodic System*; Internal Report; Free University of Amsterdam: The Netherlands, 1984.
(28) Schreckenbach, G.; Ziegler, T.; Li, J. *Int. J. Quantum Chem.* **1995**, *56*, 477.
(29) Baerends, E. J.; Ellis, D. E.; Ros, P. *Chem. Phys.* **1973**, *2*, 42.
(30) te Velde, G.; Baerends, E. J. *J. Comput. Phys.* **1992**, *99*, 94.
(31) Fonseca Guerra, C.; Visser, O.; Snijders, J. G.; te Velde, G.; Baerends, E. J. In *Methods and Techniques for Computational Chemistry*; Clementi, E., Corongiu, G., Eds.; STEF: Cagliari, 1995; p 305.
(32) Trinquier, G.; Malrieu, J.-P.; Daudey, J.-P. *Chem. Phys. Lett.* **1981**, *80*, 552.
(33) Scherer, O. J.; Winter, R.; Heckmann, G.; Wolmershäuser, G. *Angew. Chem., Int. Ed. Engl.* **1991**, *30*, 850.
(34) Muetterties, E. L.; Wright, C. M. *Q. Rev. Chem. Soc.* **1967**, *21*, 109.

Table 1. HOMO−LUMO Energy Gaps (eV), Total Energies (eV), and Relative Energies (kcal/mol) for Nine $MoAs_8^{2-}$ Isomers[a]

	LDA			PW91		
	ΔE_{HL}	E_{tot}	E_{rel}	ΔE_{HL}	E_{tot}	E_{rel}
planar (D_{8h})	0.06	−43.64	229.3	0.04	−39.20	216.9
cubic (O_h)	0.17	−45.34	190.0	0.16	−40.67	182.9
DD (D_{2d})	1.10	−49.84	86.2	1.061	−45.26	77.1
COT (D_{2d})	0.63	−51.16	55.9	0.66	−46.37	51.5
pentalene (C_{2v})	1.03	−51.46	49.0	1.01	−46.57	47.1
sandwich (D_{4h})	0.85	−51.31	52.4	1.21	−46.80	41.7
BTP (C_{2v})	1.41	−51.91	38.5	1.36	−46.90	39.3
sandwich (D_{4d})	0.95	−51.82	40.8	0.89	−47.01	36.8
crown (D_{4d})	1.69	−53.58	0.0	1.64	−48.61	0.0

[a] LDA: local density approach. PW91: generalized gradient approach using Perdew−Wang 1991 exchange−correlation functional (see refs 23−25).

contrast, the other isomers are subject to first- or second-order Jahn−Teller instability[35,36] and are only saddle points having imaginary frequencies.

The calculations reveal that the $MoAs_8^{2-}$ ion prefers an eight-coordinate crown configuration, in agreement with the experimental finding that in the $MoAs_8^{2-}$ (and $NbAs_8^{3-}$) ion the metal atom is coordinated by a crownlike As_8 cluster.[16] The crownlike configuration for $MoAs_8^{2-}$ is not surprising; in fact, the Bi_8^{2+} cluster[37] and the neutral Ch_8 (Ch = S, Se, and Te) clusters, which are isoelectronic to As_8^{8-}, all have cyclooctane-like crown configurations.[38,39] In addition, similar to the current 16-electron d^0 MAs_8^{2-} ions, the 18-electron d^2 $[Mo(CN)_8]^{4-}$ ion is also found to have an SAP structure in some crystals.[40] We will therefore discuss only the most stable (crown) geometric configuration throughout the rest of this paper.

We now consider the general structural characteristics of the MAs_8^{n-} series of complexes. In Table 2, we have listed the M−As and As−As bond lengths, nonbonding As···As distances, and AsAsAs bond angles, optimized by the LDA and PW91 methods. Both the LDA and PW91 calculations show that the M−As, As−As, and As···As distances increase from the 3d to 4d transition metal complexes by about 0.09, 0.03, and 0.15 Å, respectively. For each periodic group of transition metals, the distances of the 4d and 5d transition metal complexes are close to each other because of the *lanthanide contraction* and relativistic effects,[41−43] but they are much longer than those in the 3d transition metal complexes.

The distances of the As···As nonbonding contact in these MAs_8^{n-} ions are apparently shorter than sum of the van der Waals radii of the As atoms (about 4.0 Å),[44] implying certain interactions between As atoms not bonded directly to each other. The As···As nonbonding distances increase as M changes down the group, and decrease when M changes from group 5 to group 7. Increments of these nonbonding distances are much larger than those of the M−As and As−As distances because the "rigidity" of the As···As interactions is weak.[45]

The LDA-optimized M−As and As−As bond distances, 2.559 and 2.432 Å for $MoAs_8^{2-}$ and 2.630 and 2.463 Å for $NbAs_8^{3-}$, are in excellent agreement with the X-ray crystallographic experimental values, 2.56 and 2.429 Å for $MoAs_8^{2-}$ and 2.63 and 2.447 Å for $NbAs_8^{3-}$, respectively.[16] As usual, the optimized PW91 distances are about 0.05 Å longer than the LDA ones because of the gradient corrections. At first glance, the PW91 calculations seem to produce results worse than the LDA calculations. However, the Madelung potential between counterions in crystals and nearest-neighboring interactions, which are omitted in the present calculations for the free MAs_8^{n-} ions, could affect these distances in the solid states relative to the gas phase, as observed in polyhalogen clusters.[46] In fact, by addition of one or two alkali atoms outside the crown, the PW91 As−As bond distances improve by some 0.02 Å compared with experimental values (see below).

The optimized LDA and PW91 bond angles of AsAsAs, 90.3° and 90.5° for $MoAs_8^{2-}$ ion and 93.2° and 93.3° for $NbAs_8^{3-}$ ion, are in almost perfect agreement with the experimental values (90.6° and 93.3°, respectively) for the $MoAs_8^{2-}$ and $NbAs_8^{3-}$ crystals.[16] The optimized AsAsAs bond angles of the 3d transition metal complexes are 3−4° more acute than those of the 4d and 5d transition metal complexes; when going from the group 5 complexes to group 7 complexes, the As_8 cluster tends to contract the As−As bonds to accommodate the smaller metal atom, which causes an increase of puckering of the As_8 cavity, i.e., decrease of the AsAsAs bond angles, as noted from the experimental results.[16]

Bonding Analysis. The M−As bond lengths listed in Table 2 indicate that the M−As distances lie close to the lengths of normal single bonds,[47] indicating that the MAs_8^{n-} ions are indeed eight-coordinate complexes. Since eight-coordination is relatively uncommon for transition metal complexes, a qualitative analysis of the bonding situation in terms of the classical (localized) chemical bond approach is useful for further understanding the electronic structures of these unique ionic complexes. For the convenience of discussion, these 16-electron MAs_8^{n-} ions can be viewed as being made up of an $M^{(8-n)+}$ cation and As_8^{8-} anion. In the As_8^{8-} anion cluster, each As^- anion can have tetrahedral ("sp^3" or "p^3d") hybridization, thus rendering two σ-type As−As bonds and two lone pairs, one of which can form dative bonds with the central metal atom. From Figure 1, the dσ (d_{z^2}) orbital of the central atom will hardly be involved because of its characteristic angular orientations in the crown configuration; in fact, in a regular SAP structure, this dσ orbital is nonbonding. All the s, pσ (p_z), pπ (p_x, p_y), dπ (d_{xz}, d_{yz}), and dδ (d_{xy}, $d_{x^2-y^2}$) orbitals of the central metal atom can interact with the arsenic orbitals of proper symmetry. The central metal atom can thus be considered as "d^4sp^3" hybridization, as discussed by Kimball.[48] As a consequence of this d−s−p hybridization, eight hybrid orbitals for M−As bonding will be generated in an SAP geometry.

These qualitative analyses can be further corroborated from the viewpoint of delocalized molecular orbital (MO) theory by consideration of the symmetry properties.[49] For D_{4d} point group symmetry, the d, s, and p orbitals of the central atom will transform as $a_1 + e_2 + e_3$, a_1, and $b_2 + e_1$, respectively. The eight sets of the As 4s orbitals form 4sσ-block group orbitals ($a_1 + e_1 + e_2$) and ($b_2^* + e_3^*$), while the As 4p orbitals form

(35) Pearson, R. G. *Proc. Natl. Acad. Sci. U.S.A.* **1975**, *72*, 2104.
(36) Li, J.; Liu, C.-W.; Lu, J.-X. *J. Mol. Struct.: THEOCHEM* **1993**, *280*, 223.
(37) Beck, J.; Brendel, C. J.; Bengtsson-Kloo, L.; Krebs, B.; Mummert, M.; Stankowski, A.; Ulvenlund, S. *Chem. Ber.* **1996**, *129*, 1219.
(38) Beck, J. *Coord. Chem. Rev.* **1997**, *163*, 55.
(39) Sheldrick, W. S.; Wachhold, M. *Angew. Chem., Int. Ed. Engl.* **1995**, *34*, 450.
(40) Meske, W.; Babel, D. *Z. Naturforsch., B: Chem. Sci.* **1999**, *54*, 117.
(41) Pyykkö, P. *Phys. Scr.* **1979**, *20*, 647.
(42) Seth, M.; Dolg, M.; Fulde, P.; Schwerdtfeger, P. *J. Am. Chem. Soc.* **1995**, *117*, 6597.
(43) Küchle, W.; Dolg, M.; Stoll, H. *J. Phys. Chem. A* **1997**, *101*, 7128.
(44) Emsley, J. *The Elements*; Oxford University Press: New York, 1989.
(45) Wang, S. G.; Schwarz, W. H. E. *J. Phys. Chem.* **1995**, *99*, 11687.
(46) Li, J.; Irle, S.; Schwarz, W. H. E. *Inorg. Chem.* **1996**, *35*, 100.
(47) Orpen, A. G.; Brammer, L.; Allen, F. H.; Kennard, O.; Watson, D. G.; Taylor, R. *J. Chem. Soc., Dalton Trans., Suppl.* **1989**, S68.
(48) Kimball, G. E. *J. Chem. Phys.* **1940**, *8*, 188.
(49) Burdett, J. K.; Hoffmann, R.; Fay, R. C. *Inorg. Chem.* **1978**, *17*, 2553.

Table 2. Optimized Atomic Distances (Å) and Bond Angles (deg) for the MAs_8^{n-} Ionic Complexes[a]

	LDA				PW91			
	M−As	As−As	As···As	∠AsAsAs	M−As	As−As	As···As	∠AsAsAs
VAs_8^{3-}	2.539	2.428	3.414	89.4	2.592	2.468	3.489	89.9
$NbAs_8^{3-}$	2.640	2.459	3.576	93.2	2.685	2.500	3.637	93.3
$TaAs_8^{3-}$	2.630	2.463	3.558	92.5	2.677	2.505	3.621	92.6
$CrAs_8^{2-}$	2.464	2.404	3.292	86.4	2.516	2.442	3.368	87.2
$MoAs_8^{2-}$	2.559	2.432	3.448	90.3	2.603	2.470	3.507	90.5
WAs_8^{2-}	2.552	2.438	3.432	89.5	2.594	2.476	3.490	89.6
$MnAs_8^{-}$	2.419	2.388	3.221	84.8	2.471	2.425	3.296	85.6
$TcAs_8^{-}$	2.513	2.411	3.374	88.8	2.555	2.447	3.434	89.1
$ReAs_8^{-}$	2.515	2.421	3.375	88.4	2.556	2.457	3.432	88.6

[a] For definitions of LDA and PW91, see footnote of Table 1.

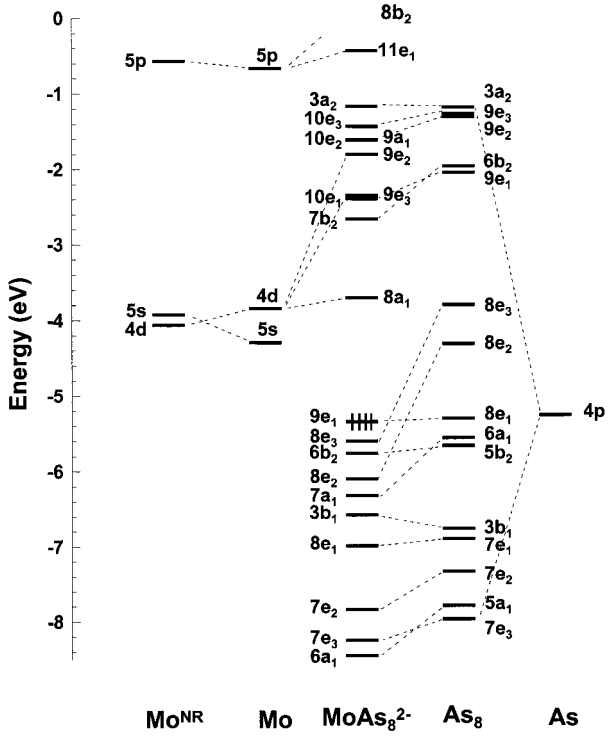

Figure 3. Energy level correlation diagram for Mo (NR: nonrelativistic) and As atoms, free As_8 ligand, and $MoAs_8^{2-}$ ion. In the center column of the $MoAs_8^{2-}$ anion, the ligand-based orbitals are labeled on the left side of the levels while the metal-based orbitals are labeled in the right side.

4pσ-block group orbitals ($a_1 + e_1 + e_2$) and ($b_2^* + e_3^*$), as well as 4pπ-block group orbitals ($a_1 + b_1 + b_2 + e_1 + e_2 + 2e_3$) and ($a_2^* + e_1^* + e_2^*$), where the asterisk indicates antibonding orbitals. The interactions between the M d orbitals and As 4p-block group orbitals will account for the major chemical interactions in these crownlike complexes.

In Figure 3 the qualitative orbital correlation is shown for the 4p-block orbitals of the free As_8 ligand, $MoAs_8^{2-}$ ion, and atomic orbitals of Mo and As atoms. All the energy levels in Figure 3 were determined by the scalar relativistic calculations except the first column (Mo^{NR}) where the nonrelativistic (NR) calculation for Mo atom was performed to provide a reference for illustrating the relativistic effects. In Figure 3, the As 4p orbitals in the free As_8 ligand span all the orbitals from $7e_3$ up to the $3a_2$ representations, with $8e_3$ orbitals being the highest SOMOs (singly occupied MOs). The Mo 5s and 4d orbitals, slightly affected by the *direct* and *indirect relativistic effects*,[50−53] can interact efficiently with the 4p-block group orbitals.

For the D_{4d} crown complexes, the eight sets of As^- 4s orbitals form the $5a_1$, $7e_1$, $6e_2$, $6e_3$, and $5b_2$ MOs, which are separated fairly well from the "frontier" MOs ($6a_1$ and up) formed by the As 4p orbitals and Mo 4d−5s−5p orbitals. In the $MoAs_8^{2-}$ anion, the 32 electrons from the eight sets of As^- $4p^4$ manifold fill up all the 16 4pσ- and 4pπ-block orbitals from $6a_1$ to $9e_1$ (HOMO), thus leaving the 4pσ* and 4pπ* orbitals unoccupied. It should be pointed out that the electrostatic shifting on the eigenvalues of the $MoAs_8^{2-}$ dianion has been corrected in Figure 3 to compare the ionic energy levels with the neutral systems; all the eigenvalues of $MoAs_8^{2-}$ ion have been shifted down by 7.5 eV so that the centers of the 3d-, 4s-, and 4p-block MOs can roughly match the orbital energies of As 3d, 4s, and 4p atomic orbitals.

When the Mo atom is encapsulated in the center of the As_8 crown, all the ligand orbitals with a_1, e_2, and e_3 symmetries are markedly stabilized because of their covalent interactions with the Mo 5s−4dσ, dδ, and dπ orbitals. This can be seen from the central column of Figure 3. The eigenvalues of the $6a_1$ (18% 5s of Mo, same in below), $7a_1$ (23% 5s + 23% 4dσ), $7e_2$ (21% 4dδ), $7e_3$ (18% 4dπ), $8e_2$ (27% 4dδ), and $8e_3$ (41% 4dπ) MOs are all lowered relative to those of the corresponding orbitals in the free As_8 ligand. In contrast, the Mo dδ and dπ orbitals have been markedly destabilized as a consequence of the strong covalent interactions with e_2 and e_3 ligand group orbitals.

As mentioned previously, owing to its orientation, the dσ orbital has little overlap with the ligands. As a result, the $8a_1$ orbital (70% dσ), which is only slightly influenced by the ligands, becomes the lowest unoccupied molecular orbital (LUMO) and could play an important role in formation of 18-electron d^2 complexes. Prior qualitative analysis anticipates that in a typical SAP structure the d orbitals split as d$\sigma \ll$ d$\delta <$ dπ, indicating a larger orbital interaction for dπ orbitals than for the dδ orbitals.[49] In the present case, the interaction of dδ−e_2 is almost as strong as that of dπ−e_3 because of compression in the SAP structure (Figure 1), which leads to an increase in orbital overlap between the dδ orbitals and the ligand group orbitals.

Spin−Orbit Coupling Effects. Since the SO coupling constants increase from group 5 to group 7 and from the 3d to 5d transition metals,[54] it is particularly crucial to explore SO effects on the electronic structures of complexes involving the 5d transition metals. We therefore examined the Re-containing complex, which presumably has the largest SO effects among this series of complexes.

From our calculation on the Re atom, scalar relativistic effects destabilize the 5d orbitals by 1.57 eV but stabilize the 6s orbital

(50) Pitzer, K. S. *Acc. Chem. Res.* **1979**, *12*, 271.
(51) Pyykkö, P.; Desclaux, J.-P. *Acc. Chem. Res.* **1979**, *12*, 276.
(52) Pyykkö, P. *Chem. Rev.* **1988**, *88*, 563.
(53) Schwarz, W. H. E.; van Wezenbeek, E. M.; Baerends, E. J.; Snijder, J. G. *J. Phys.* **1989**, *B22*, 1515.
(54) Gerloch, M. *Orbitals, Terms and States*; John Wiley & Sons: Chichester, 1986.

Table 3. Mulliken Overlap Populations, Net Charges, and Atomic Configurations for the MAs_8^{n-} Ionic Complexes

	overlap population			net charge (configuration)[a]	
	M−As	As−As	As···As	M	As
VAs_8^{3-}	0.28	0.34	−0.19	0.58 ($d^{3.7}s^{0.3}p^{0.4}$)	−0.45
$NbAs_8^{3-}$	0.10	0.42	−0.18	1.57 ($d^{3.1}s^{0.5}p^{0.0}$)	−0.57
$TaAs_8^{3-}$	−0.26	0.46	−0.14	1.15 ($d^{2.9}s^{0.9}p^{0.1}$)	−0.52
$CrAs_8^{2-}$	0.33	0.43	−0.12	0.31 ($d^{4.8}s^{0.3}p^{0.6}$)	−0.29
$MoAs_8^{2-}$	0.20	0.48	−0.12	1.30 ($d^{4.2}s^{0.4}p^{0.1}$)	−0.41
WAs_8^{2-}	−0.89	0.66	−0.02	1.03 ($d^{4.0}s^{0.7}p^{0.3}$)	−0.38
$MnAs_8^{-}$	0.35	0.49	−0.07	0.09 ($d^{5.8}s^{0.3}p^{0.8}$)	−0.14
$TcAs_8^{-}$	0.27	0.53	−0.07	0.95 ($d^{5.3}s^{0.4}p^{0.3}$)	−0.24
$ReAs_8^{-}$	−0.40	0.63	−0.01	0.74 ($d^{5.1}s^{0.7}p^{0.4}$)	−0.22

[a] The atomic configurations of As atom ($s^{1.8-1.9}p^{3.1-3.5}d^{0.15-0.18}$) are hardly changed.

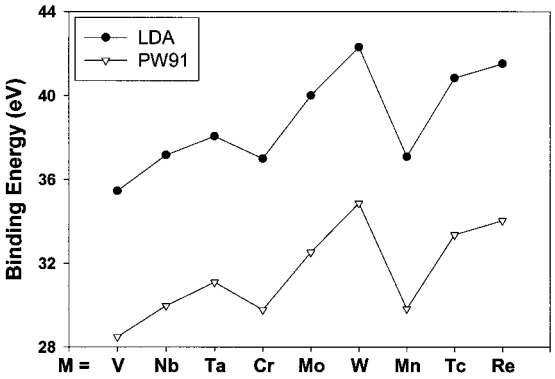

Figure 4. LDA and PW91 atomization energies of MAs_8^{n-} (M = V, Nb, Ta, Cr, Mo, W, Mn, Tc, Re) ions.

by 1.09 eV. By inclusion of SO coupling, the Re 6s orbital is slightly stabilized (0.06 eV), whereas the 5d and 6p orbitals are split by 0.81 and 0.75 eV, respectively. For the As atom, scalar relativistic effects stabilize the 4s orbital by 0.47 eV but destabilize the 4p orbitals only marginally (0.03 eV). The As 4s orbital is slightly destabilized (0.08 eV), while the 4p orbitals are split by 0.28 eV with inclusion of the SO coupling effects.

The energy levels of the $ReAs_8^-$ are, not surprisingly, akin to those of the $MoAs_8^{2-}$ (see Figure 3). When the scalar relativistic effects are taken into account, the $8a_1$, $9e_3$, $9e_2$ and $9a_1$ orbitals are affected markedly because they consist mainly of Re 6s and 5d orbitals. The ligand-based orbitals (e.g., $6b_2$, $9e_1$, $7b_2$, $10e_1$, $10e_2$, $3a_2$, and $10e_3$) are almost unaffected by inclusion of scalar relativistic effects and SO effcets, as expected. However, when SO effects are included, the large Re 5d contributions to the $8e_2$, $8e_3$, $9e_3$, and $9e_2$ orbitals warrant the largest SO splitting for these MOs. Quantitatively, the two occupied $8e_2$ and $8e_3$ MOs are split by about 0.29 eV, while the virtual orbitals $9e_3$, $9e_2$, $10e_2$, and $10e_3$ are split by 0.17, 0.12, 0.09, and 0.01 eV, respectively. Therefore, SO effects for ground states of these complexes are indeed small because the first-order SO effects should be zero for ground states of closed-shell systems.[55] The scalar relativistic effects account for the most crucial relativistic effects on structures and bonding, whereas SO effects are expected to be even smaller. We have therefore ignored the influence of such effects on ground-state geometries and vibrational properties.

Relative Stabilities. The bonding analysis indicates that there are crucial orbital overlaps between metal d orbitals and As 4p orbitals, and all the early transition metal polyarsenic complexes under consideration can exist as diamagnetic, closed-shell systems with large HOMO−LUMO energy gaps. The relative stabilities of these free ions will be addressed on the basis of the interatomic Mulliken overlap populations (Table 3)[56] and the calculated atomization energies (Figure 4).[57]

Although the M−As overlap populations are negative for the 5d transition metal complexes because of the basis set dependency of the Mulliken population analysis,[58,59] the trend in the series of MAs_8^{n-} ions is nonetheless evident. Within each group of transition metals, the M−As overlap populations decrease, whereas those of the As−As increase when going from the 3d to 5d transition metal complexes. When going from the group 5 to group 7 complexes, the overlap populations increase for both M−As and As−As bonds. This is in agreement with the calculated MAs_8^{n-} atomization energies, which increase when the transition metal changes from group 5 to group 7 and from the first row to the third row.

The variations of the bonding strengths and atomization energies can be related to the covalent bonding between metal d-type orbitals and As 4p orbitals, which is enhanced when their orbital energies become closer to each other. From group 5 to group 7, the metal d orbital energies decrease because of increasing effective nuclear charges and become closer in energy to those of the As 4p orbitals. However, in going from the 3d to 5d metals, although the metal d orbital energies in each group increases, giving rise to a decrease of the M−As overlap populations, the As−As interaction is markedly strengthened, thus causing a net increase of atomization energy.

From the bonding strengths and atomization energies, one can conclude that the As_8 complexes of the group 7 transition metals are the most stable ones among the three groups of complexes. Therefore, an experimental synthesis of stable $ReAs_8^-$ complex seems feasible. The $TaAs_8^{3-}$ and WAs_8^{2-} complexes are also practical targets for the synthesis.

Charge Distribution and Reactivities. As listed in Table 3, the net charges, q_M and $|q_{As}|$, decrease for MAs_8^{n-} complexes on going from group 5 to group 7 transition metals, in agreement with the increasing covalent interactions. Although the transition metals can be formally viewed as d^0 centers having the highest possible oxidation states, the actual net charges they carry all lie between 0 and +2 on the basis of the Mulliken analysis. The electronic configurations show that whereas the electron populations of the As orbitals are hardly changed with alteration of the central metals, those of the metal atoms indeed change markedly. For instance, the metallic d orbital populations increase by about $1e^-$ when M goes from group 5 to group 6 and from group 6 to group 7, and they decrease by 0.6 and 0.2 e^-, respectively, when M changes from 3d to 4d and from 4d to 5d transition metals. The charge populations and electronic configurations indicate that the As_8^{8-} ion has strong electron donations to the metal center via covalent interactions.

To illustrate these covalent interactions between the ligand and metal atom, we have shown in Figure 5 the stereocontour diagrams for the frontier MOs from $7a_1$ to $8a_1$ (LUMO). Among these MOs, the $8a_1$ orbital is mostly a pure metallic dσ orbital, while the $7a_1$, $8e_2$, and $8e_3$ orbitals account for the major metal−ligand covalent interactions (see Figure 3). The low-lying and nearly nonbonding nature of the $8a_1$ orbital paves the way for accepting electron donations or accommodating up to two additional electrons to form d^2 complexes, which seems feasible

(55) Richards, W. G.; Trivedi, H. P.; Cooper, D. L. *Spin−Orbit Coupling in Molecules*; Clarendon Press: Oxford, 1981.
(56) Mulliken, R. S. *J. Chem. Phys.* **1955**, *23*, 1833.
(57) Baerends, E. J.; Branchadell, V.; Sodupe, M. *Chem. Phys. Lett.* **1997**, *265*, 481.
(58) Wiberg, K. B.; Rablen, P. R. *J. Comput. Chem.* **1993**, *14*, 1504.
(59) Meister, J.; Schwarz, W. H. E. *J. Phys. Chem.* **1994**, *98*, 8245.

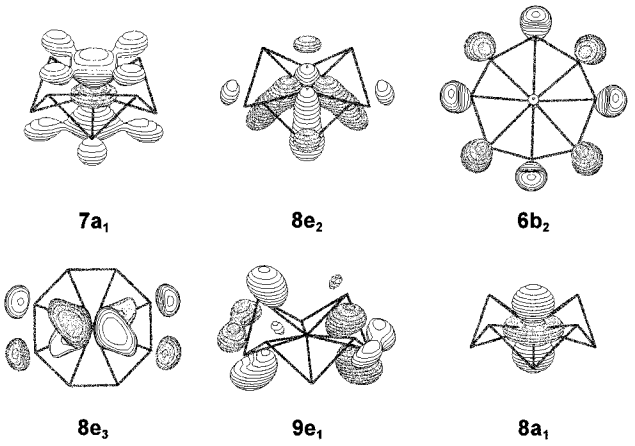

Figure 5. Contour diagram of the six important frontier orbitals ($7a_1$, $8e_2$, $6b_2$, $8e_3$, $9e_1$, and $8a_1$) for $MoAs_8^{2-}$ ion. The contours are at intervals of 0.0125, and the solid (dashed) line represents the positive (negative) contours of the wave functions.

for late transition metal complexes. It is evident from Figure 5 that the $8e_2$ and $8e_3$ MOs have strong bonding participation of the Mo dδ and dπ orbitals, while the $7a_1$ MO has direct bonding interaction between the Mo 5s−dσ and As 4p orbitals.

One of the most interesting features of this $7a_1$ MO is that the four As atoms at either side of the crown have formed a region of high electron density outside the crown. As a consequence, this region has become highly reactive toward cations, such as alkali metal ions. It is this orbital that makes the MAs_8^{n-} anion behave like an η^4 (tetrahepto) electron-donating ligand. This explains why the $MoAs_8^{2-}$ and $NbAs_8^{3-}$ anions can coordinate to large-size alkali metals such as K, Rb, and Cs in solutions [16] or form the one-dimensional $_\infty^1[Rb \cdot NbAs_8]^{2-}$ chain in the solid-state.[18] The calculations of $[MMoAs_8]^-$ and $[M_2MoAs_8]$ (M = Li, Na, K, Rb, and Cs) indicate that the major interaction lies between the As 4pσ orbital and the M *n*s and *n*p$_z$ orbitals.[60] This results in a noticeable stabilization of the $7a_1$ orbital (e.g., 12% in Rb_2MoAs_8), while the $8a_1$ orbital (5%) does not change much. On the other hand, the occupied frontier MOs, $6b_2$ and $9e_1$, are almost purely ligand-based orbitals and they are practically nonbonding with regard to the metal−ligand interactions. Although these MOs can in principle be useful for donating electrons to other empty orbitals, calculations of the above mono- and dialkali compounds indicate little interaction between the alkali atoms and the $MoAs_8^{2-}$ ligands (less than 4%) in the $6b_2$ and $9e_1$ orbitals.

Vibrational Properties. The 18 vibrational modes ($2A_1 + B_1 + B_2 + 2E_1 + 3E_2 + 2E_3$) of the As_8 cluster are augmented in MAs_8^{n-} ion by three more modes ($B_2 + E_1$), which correspond to translations of the central metal atom in the As_8 cavity. Among these vibrations, the B_2 and E_1 modes are IR-active, while the A_1, E_2, and E_3 modes are Raman-active.[61] Table 4 lists the calculated vibrational frequencies and IR absorption intensities[62] of As_8 and MAs_8^{2-} (M = Cr, Mo, W).

From Table 4, the free As_8 cluster has only three IR-active bands and the intensities of these bands are extremely weak, as is found for the Se_8 cluster.[63] The encapsulation of a metal atom in the As_8 cluster increases all low frequencies and IR intensities. The two A_1 modes are breathing vibrations of the As_8 crown, where $1A_1$ is the *x*,*y*-direction breathing and $2A_1$ is the compression in the *z*-direction. Since the central atom lies in the center of these fully symmetric vibrations, one can directly compare the A_1 frequencies without consideration of the difference in reduced masses. It is not surprising that the frequency of the $1A_1$ mode increases from As_8 to the 3d, 4d, and 5d MAs_8^{n-} complexes, implying that the As_8 crown becomes harder to breath in the *x* and *y* directions upon bonding to a central metal atom. In contrast, the *z*-direction compression becomes easier for MAs_8^{2-} than for the free As_8 cluster.

Table 4. Calculated LDA Vibrational Frequencies (cm^{-1}) and IR Absorption Intensities (km/mol, in Parentheses) for As_8 and MAs_8^{2-} (M = Cr, Mo, and W) Ions[a]

mode	As_8	$CrAs_8^{2-}$	$MoAs_8^{2-}$	WAs_8^{2-}
$1A_1$	112	143	153	162
$2A_1$	312	297	287	281
$1B_2$	109 (0.2)	103 (3.7)	92 (2.9)	103 (3.2)
$2B_2$		309 (10.2)	270 (4.4)	235 (2.0)
$1E_1$	70 (1.4)	96 (3.6)	93 (5.4)	96 (2.8)
$2E_1$	299 (0.8)	269 (38.4)	243 (23.6)	218 (2.6)
$3E_1$		389 (1.0)	342 (10.4)	304 (35.8)
$1E_2$	33	82	86	87
$2E_2$	80	135	146	150
$3E_2$	269	266	259	260
$1E_3$	104	131	144	148
$2E_3$	256	243	233	235

[a] For definition of LDA, see footnote of Table 1.

There are several trends worthy of comment. (1) All IR intensities of the gas-phase MAs_8^{n-} ions decrease considerably as M changes from group 5 to group 7, since the larger negative charges lead to a greater change of the derivatives of dipole moments during the vibrations. (2) From the 3d to the 5d transition metals, except for the $1E_1$ and $1B_2$ modes, the frequencies decrease for all other IR modes, $2E_1$, $3E_1$, and $2B_2$, in agreement with the increasing reduced masses of these modes when the metal becomes heavier. (3) The intensities of the $2E_1$ (and $2B_2$) modes decrease significantly, whereas those of the $3E_1$ modes increase accordingly when going across the series of 3d, 4d, and 5d metals. The $2B_2$ and $3E_1$ modes are mainly the *z*- and *x*,*y*-direction translation modes of the metal atom in the crown cavity. These changes of frequencies and intensities therefore reflect the interaction between the M atom and As_8 cavity. The intensity increase of the $3E_1$ mode benefits from the stronger coupling with the *z*-direction stretching mode (mainly $2E_1$) when the metal becomes heavier.

Stabilities of MoA_8^{2-} (A = N, P, Sb, and Bi) Pnictide Ions. Finally, we want to explore whether the analogous crownlike complexes could possibly exist for the other pnicogen elements N, P, Sb, and Bi. The calculated total energies and atomization energies for the MoA_8^{2-} complexes for the process of $MoA_8^{2-} \rightarrow Mo + 6A + 2A^-$ are listed in Table 5. Because of the lack of f-type polarization functions for all the pnicogen elements, triple-ζ basis sets with d-type polarization functions were used for these calculations.

From Table 5, the atomization energies of these complexes decrease regularly when the pnicogen atom becomes heavier from P to Bi. Since the N_2 molecule is an extremely stable entity, one has to compare the stability of the MoN_8^{2-} complex with that of the isolated dinitrogen as well. The energy changes were calculated for the decomposition reaction process $MoA_8^{2-} \rightarrow Mo + 3A_2 + A_2^{2-}$. The decomposition reaction energies (E_{rxn}) are also listed in Table 5. It turns out that decompositions of all the MoP_8^{2-}, $MoAs_8^{2-}$, $MoSb_8^{2-}$, and $MoBi_8^{2-}$ complexes

(60) Li, J.; Wu, K. C. Unpublished results.
(61) Cotton, F. A. *Chemical Applications of Group Theory*, 3rd ed.; Wiley: New York, 1990.
(62) Wilson, E. B.; Decius, J. C.; Cross, P. C. *Molecular Vibrations*; McGraw-Hill: New York, 1955; p 163.
(63) Kohara, S.; Goldbach, A.; Koura, N.; Saboungi, M.-L.; Curtiss, L. A. *Chem. Phys. Lett.* **1998**, *287*, 282.

Table 5. PW91 Total Energies, Atomization Energies, and Decomposition Reaction Energies of MoA_8^{2-} (A = N, P, As, Sb, and Bi)[a]

	E_{tot}	E_{atom}	E_{rxn}
MoN_8^{2-}	−62.43	36.16	2.94
MoP_8^{2-}	−52.89	35.62	17.33
$MoAs_8^{2-}$	−48.04	31.95	16.71
$MoSb_8^{2-}$	−42.06	27.70	15.61
$MoBi_8^{2-}$	−40.02	26.22	14.95

[a] All energies are in eV. For definition of PW91, see footnote of Table 1.

are endothermic, with the endothermocity decreasing from MoP_8^{2-} to $MoBi_8^{2-}$. One can conclude from these reaction energies that the thermodynamic stabilities of the MoA_8^{2-} (A = P, As, Sb, and Bi) complexes decrease from P to Bi, which is in accordance with the tendency inferred from the calculated atomization energies.

However, even though the MoN_8^{2-} ion has the largest atomization energy in this series of ionic complexes, the decomposition of MoN_8^{2-} tends to be much less endothermic than the other analogues; its PW91 decomposition energy is only about 3 eV. In fact, the frequency calculations indicate that the MoN_8^{2-} species with the SAP structure is only a higher-order saddle point on the potential energy surface. Therefore, the crownlike MoN_8^{2-} complex is not stable. Calculations on other MoN_8^{2-} isomers indicate that the SAP structure is energetically higher than the dodecahedron, bicapped trigonal prism (BTP), and staggered sandwich structures by 8.49, 3.50, and 1.51 eV, respectively!

In contrast, all the MoA_8^{2-} (A = P, As, Sb, and Bi) ions are indeed real mimima, with the lowest vibrational frequencies decreasing from 123, 85, and 52 to 39 cm^{-1} for A = P, As, Sb, and Bi, respectively. For MoA_8^{2-} (A = N, P, As, Sb, and Bi), the frequencies of the *x*,*y* breathing modes ($1A_1$) decrease as 623, 268, 152, 96, and 71 cm^{-1}, while those of the *z*-direction compressing modes decrease as 805, 463, 258, 204, and 153 cm^{-1}, respectively. Hence, it is apparent that the interaction between the central atom and A_8 cavity decreases when the pnicogen elements become heavier. It thus seems reasonable to be able to synthesize the MoP_8^{2-} and $MoSb_8^{2-}$ ions. The similar CoP_8^{+} and NiP_8^{+} cations have been identified in recent laser-ablation experiments.[64]

Concluding Remarks

The As_8^{8-} cluster, isoelectronic and isostructural to the S_8 and Se_8 homocyclic clusters, can form a crownlike geometry with a metal atom in the center. In this paper, we have examined the geometries, electronic structures, spin−orbit coupling effects, and properties such as thermodynamic stabilities and vibrational frequencies of the MAs_8^{n-} series of complexes. The levels of metal-containing orbitals indeed split noticeably when the SO coupling is taken into account, but the splittings are not important for the ground-state properties. The computational simulations of the vibrational spectra of these complexes have laid the foundation for future experimental comparison.

For the MAs_8^{n-} series of ions, the tendency of changes can be summarized as follows. (1) For the same row of transition metals, the M−As and As−As distances and AsAsAs bond angles steadily decrease from group 5 to group 7 transition metal complexes. Accordingly, the M−As and As−As overlap populations all increase and the net charges q_M and $|q_{As}|$ decrease. These changes reflect the enhanced covalent interaction in these complexes, as is shown by the noticeable increase of the atomization energies. (2) Within the same periodic group, from the 3d to 4d (or 5d) transition metal complexes, the M−As and As−As distances, AsAsAs bond angles, and net charges q_M and $|q_{As}|$ all considerably increase, consistent with the expanded atomic size. Although the M−As overlap populations decrease because of the increasing M−As distances, the As−As bonding interactions are remarkably increased, which overcompensate the energy loss due to the decrease of the M−As bonding strengths. As a result, the stability increases from the 3d to the 4d and 5d complexes, as indicated by the atomization energies and decomposition reaction energies.

The analogous pnictide ion complexes of MoA_8^{2-} (A = P, Sb, Bi) are found to be thermodynamically stable as well; they have large atomization energies and their decompositions are also highly endothermic. These complexes together with the $TaAs_8^{3-}$, WAs_8^{2-}, and $ReAs_8^{-}$ complexes constitute potential targets for the synthesis. Although we focus on the early transition metal polyarsenic complexes, theoretical exploration of the polyarsenic and polyphosphides complexes of the late transition metals could also be interesting. Our research of this problem is in progress.

Acknowledgment. We acknowledge the State Key Laboratory of Structural Chemistry of China for financial support and Fujian Institute of Research on the Structure of Matter, Chinese Academy of Sciences for computer time. We are also grateful to the reviewers for their valuable suggestions. J.L. thanks Professor Huang Jin-Shun for the hospitality during his visit to the Fujian Institute.

IC9902166

(64) Greenwood, P. F.; Dance, I. G.; Fisher, K. J.; Willett, G. D. *Inorg. Chem.* **1998**, *37*, 6288.